DREAMS: Preserving both Local and Global Structure in Dimensionality Reduction

Anonymous authors
Paper under double-blind review

Abstract

Dimensionality reduction techniques are widely used for visualizing high-dimensional data in two dimensions. Existing methods are typically designed to preserve either local (e.g. t-SNE, UMAP) or global (e.g. MDS, PCA) structure of the data, but none of the established methods can represent both aspects well. In this paper, we present DREAMS (Dimensionality Reduction Enhanced Across Multiple Scales), a method that combines the local structure preservation of t-SNE with the global structure preservation of PCA via a simple regularization term. Our approach generates a spectrum of embeddings between the locally well-structured t-SNE embedding and the globally well-structured PCA embedding, efficiently balancing both local and global structure preservation. We benchmark DREAMS across eleven real-world datasets, showcasing qualitatively and quantitatively its superior ability to preserve structure across multiple scales compared to previous approaches.

1 Introduction

Real-world data often exhibits high-dimensional and complex structures, making their effective and interpretable visualization a crucial step in exploratory data analysis. Dimensionality reduction methods serve this purpose by projecting high-dimensional data into more interpretable low-dimensional representations while preserving meaningful structures. Among dimensionality reduction methods, principal component analysis (PCA, Hotelling 1933) and t-distributed stochastic neighbor embedding (t-SNE, van der Maaten and Hinton 2008) have emerged as two widely used methods, each with distinct strengths. PCA excels at capturing global structures by projecting data onto a lower-dimensional subspace in directions that maximize variance, providing a broad overview of the dataset's structure. In contrast, t-SNE is a neighbor-embedding method with the objective to map data points that are nearby in high-dimensional space close to one another in the low-dimensional embedding. Its focus on neighborhood preservation makes t-SNE particularly effective in preserving local structures. When applied individually, both methods suffer from limitations: PCA often overlooks fine local relationships, while t-SNE distorts global structures in favor of local neighborhood preservation.

However, in many real-world datasets, e.g. single-cell transcriptomic datasets, both local and global structure is meaningful. Local relationships can reveal microscopic data patterns such as small clusters and cell types. For example, the Tasic et al. dataset features 122 fine clusters that represent cell types, which are clearly separated in the t-SNE plot (Figure 1 right). Conversely, the global structure reflects macroscopic data patterns such as separations between broad cell classes (Tasic et al., 2018) or developmental trajectories (Kanton et al., 2019) across an entire cell population. In the Tasic et al. dataset, this level of structure separates individual cells into non-neurons, excitatory, and inhibitory neurons. This global structure is not evident in the t-SNE plot, but is prominent in the PCA visualization, which in turn fails to separate the finer clusters (Figure 1 left). Since both local and global structure carry essential and often complementary information, neglecting either structure scale can result in incomplete or biased interpretations, highlighting the importance of preserving both scales simultaneously.

Our proposed method DREAMS combines the interpretability and global structure preservation of PCA with the local sensitivity of t-SNE in a simple, yet effective way. On the Tasic et al. data, it maintains

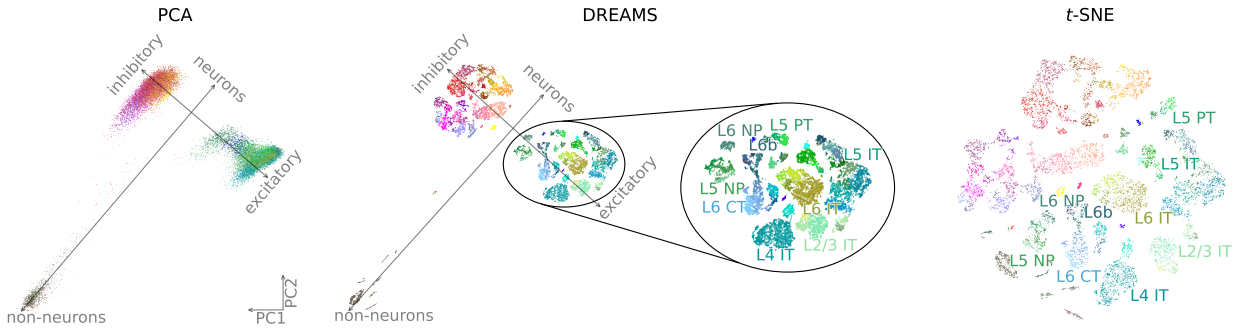

Figure 1: PCA, DREAMS, and t-SNE embeddings of the Tasic et al. dataset (Tasic et al., 2018) illustrate how DREAMS preserves the global organization seen in the PCA embedding — such as the separation of non-neurons, inhibitory, and excitatory neurons — while also capturing the local cell-type structure that is present in the t-SNE embedding.

PCA's global arrangement by non-neurons, inhibitory, and excitatory neurons, while also revealing the finer cluster structure within each broad group, similar to t-SNE (Figure 1 middle). DREAMS integrates global structure preservation into the t-SNE objective by a PCA-based regularization term applied throughout the entire optimization process. Varying the regularization strength allows DREAMS to transition from the locally well-structured t-SNE embedding to the globally well-structured PCA embedding. Along this spectrum it trades off local and global structure more favorably than its competitors resulting in improved qualitative and quantitative structure preservation, particularly on datasets with hierarchical organization that exhibit both prominent local and global patterns.

We chose PCA as the default global method in DREAMS due to its simplicity, inherent interpretability (PCA is linear) and fast runtime. That said, DREAMS also offers regularizing with other global embeddings such as multidimensional scaling (MDS).

In summary, we introduce the new method DREAMS making the following contributions:

1. suggest a simple but effective regularization strategy to combine t-SNE's local with PCA's global quality;
2. present a spectrum of visualizations from t-SNE to PCA with almost no local/global structure trade-off;
3. perform a benchmark of ten algorithms on eleven real-world datasets;
4. provide an open-source implementation of DREAMS based on the `openTSNE` library.

Our code to reproduce the results of this paper is provided as supplementary material and will be made publicly available upon acceptance. We used a modified openTSNE implementation (supplementary folder DREAMS) and a modified CNE implementation (supplementary folder DREAMS-CNE).

2 Related Work

The most prominent and well-established visualization methods either excel at preserving local structure, e.g., neighbor-embedding methods, such as t-SNE (van der Maaten and Hinton, 2008) and UMAP (McInnes et al., 2018), or global structure such as PCA (Pearson, 1901; Hotelling, 1933) and MDS (Kruskal, 1964), but not both simultaneously. Therefore, many recent efforts have aimed at producing visualizations with faithful local *and* global structure.

Most of them attempt to improve the global structure preservation of neighbor embeddings. One way to make neighbor embeddings more sensitive to the global structure of a dataset is to widen the set of points that are deemed similar beyond a small set of nearest neighbors. For instance, increasing the perplexity parameter in t-SNE effectively increases the number of considered nearest neighbors but consequently leads to increased runtime (Kobak and Berens, 2019; Lee et al., 2015; De Bodt et al., 2020). Similarly, several modifications of UMAP, e.g. PaCMAP (Wang et al., 2021) and TriMAP (Amid and Warmuth, 2019), do

not only use nearest neighbors, but also consider more distant points in their optimization. In addition to attraction between nearest neighbors, PaCMAP employs weak attraction on mid-near points, while TriMap tries to also preserve the order of similarities in random triplets. Another triplet-based method, ivis (Szubert et al., 2019), strives to balance local and global structure with a parametric encoder and a margin loss on triplets of embedding distances.

A different strategy to improve the global structure in neighbor embeddings is to initialize them with a global embedding, which can improve the global structure of the final embedding, despite no further steps for preserving global structure during optimization (Kobak and Linderman, 2021; Wang et al., 2021).

A prominent way to trade off local and global structures within the neighbor-embedding framework is the attraction-repulsion spectrum (Böhm et al., 2022; Damrich et al., 2023). Along this spectrum methods with stronger between-neighbor attraction tend to focus on more global structure. UMAP and t-SNE both lie on this spectrum with UMAP having more attraction. The most global method on this attraction-repulsion spectrum is Laplacian Eigenmaps (Belkin and Niyogi, 2003).

Recently, hybrid methods were proposed that combine elements of neighbor embedding methods and global methods during optimization. Several of these are variational autoencoders with a 2D latent space and regularized ELBO maximization. The method scvis (Ding et al., 2018) uses a Gaussian latent prior and adds a variant of the t-SNE objective to the ELBO. Its successor VAE-SNE (Graving and Couzin, 2020) employs a more flexible Gaussian mixture prior. Instead of a regularizer promoting local structure preservation, ViVAE (Novak et al., 2023) adds a stochastic MDS regularizer, but denoises the high-dimensional data based on k-nearest neighbor relations.

More similar to our approach are non-parametric hybrid methods that directly optimize the embedding positions. Local-to-Global Structures (Miller et al., 2023), a method for generic graph drawing, applies MDS-like stress minimization to shortest path graph distances among pairs of points that are strongly connected, while repelling non-neighboring pairs. The SQuadMDS-hybrid (Lambert et al., 2022) interpolates between the objectives of t-SNE and MDS. For MDS it uses the stochastic quartet framework of Lambert et al. (2022). To make both objectives more compatible, SQuadMDS-hybrid normalizes their gradients before blending them together. The hybrid method StarMAP (Watanabe et al., 2025) changes the attractive force in the UMAP objective. Instead of pulling only nearest neighbors together, it also pulls points towards the PCA coordinates of their k-means cluster centroid. This combination of a neighbor embedding with PCA is similar to our DREAMS. But instead of UMAP, we use t-SNE due to its better local structure preservation. Moreover, we propose a simpler objective that avoids StarMAP's clustering step, leaves the neighbor-embedding objective intact, and simply pulls each embedding point towards its own PCA position. We found that this simpler approach leads to a better local-global trade-off. Additionally, setting the regularization strength in DREAMS to 0 or to 1 allows to recover standard t-SNE and PCA, while the StarMAP framework cannot fully recover PCA.

Different from neighbor-embedding-inspired methods, PHATE (Moon et al., 2019) is a diffusion-based method that tries to balance local and global structure preservation. Like neighbor embeddings, it starts with the k-nearest neighbor graph of the high-dimensional data. It then integrates this local information into a global graph distance. PHATE uses potential distance, a variant of diffusion distance that focuses more on global structure. To visualize this global distance metric in 2D, PHATE uses MDS. Geometry-regularized autoencoders of Duque et al. (2022) regularize their 2D latent space with a precomputed PHATE embedding. DREAMS also uses a reference embedding for regularization, but is non-parametric, uses PCA or MDS, and employs the t-SNE loss instead of the reconstruction loss.

3 Background

In dimensionality reduction, we aim to represent a high-dimensional dataset $X = [x_1, \dots, x_n]^T \in \mathbb{R}^{n \times m}$ with n observations in an m-dimensional space by a lower-dimensional embedding $Y = [y_1, \dots, y_n]^T \in \mathbb{R}^{n \times d}$, where $d \ll m$. The objective is to construct Y such that meaningful relationships among the observations are preserved in the lower-dimensional space. In this section, we outline the two dimensionality reduction

methods that DREAMS builds upon — PCA and t-SNE — and show how they approach this goal from complementary perspectives.

3.1 Principal component analysis (PCA)

Principal component analysis (PCA; Pearson 1901; Hotelling 1933) is a linear transformation that projects the data onto a new coordinate system aligned with the directions of maximum variance. PCA seeks a linear, orthogonal mapping $W \in \mathbb{R}^{m \times d}$ that projects the data into a lower-dimensional space $Y = XW$, where the directions in W capture the maximal variance across the entire dataset X. This ensures the preservation of the macroscopic, global structure since distances along directions with high variance are preserved in the projection (Huang et al., 2022). However, because orthogonal projections can map distant points to similar locations, PCA performs poorly at preserving local structures (Huang et al., 2022; Wang et al., 2023).

3.2 t-distributed stochastic neighbor embedding (t-SNE)

t-distributed stochastic neighbor embedding (t-SNE; van der Maaten and Hinton 2008) is a widely used neighbor embedding method, that is especially effective at preserving local similarities (Espadoto et al., 2019). By transforming Euclidean distances between points into pairwise similarity probabilities, t-SNE constructs a probability distribution, P, based on the high-dimensional observations X, and a probability distribution, Q, based on the low-dimensional embeddings Y. The distribution $P = \{p_{ij}\}_{i,j=1}^{n}$ encodes the nearest-neighbor structure in the high-dimensional space via

$$p_{ij} = \frac{p_{j|i} + p_{i|j}}{2n}, \text{ where } p_{j|i} = \frac{\exp\left(-\|x_i - x_j\|^2/(2\sigma_i^2)\right)}{\sum_{k \neq i} \exp\left(-\|x_i - x_k\|^2/(2\sigma_i^2)\right)} \text{ if } i \neq j \text{ and } p_{i|i} = 0.$$

The width σ_i of the Gaussian kernels is adaptively chosen for each data point to ensure the same effective neighborhood size, i.e., the number of points j for which $p_{j|i} \gg 0$. Due to the exponential decrease of the Gaussians, most p_{ij} are close to zero, and are treated as exactly zero in most implementations.

The similarity probability distribution of the low-dimensional embedding points, $Q = \{q_{ij}\}_{i,j=1}^{n}$, is based on a Cauchy kernel:

$$q_{ij} = \frac{\left(1 + \|y_i - y_j\|^2\right)^{-1}}{\sum_{k \neq l} \left(1 + \|y_k - y_l\|^2\right)^{-1}} \text{ if } i \neq j \text{ and } q_{ii} = 0.$$

The objective is to arrange the low-dimensional embedding Y such that the low-dimensional similarities q_{ij} match the similarities p_{ij} as measured by the Kullback–Leibler divergence

$$\mathcal{L}_{t\text{-SNE}}(Y) = \mathrm{KL}(P \parallel Q) = \sum_{i,j} p_{ij} \log \frac{p_{ij}}{q_{ij}}, \tag{1}$$

which is minimized via gradient descent with respect to the embedding positions Y.

The similarity probabilities act as kernels centered around the data and embedding points, assigning high similarity values only to close neighbors while distant points have little impact on the loss function. This makes neighbors in the high-dimensional space remain neighbors in the low-dimensional embedding space, ensuring the preservation of local structure. In contrast, due to the weak influence of distant points, global structure can be misrepresented (Huang et al., 2022; Wang et al., 2023).

4 Methods

4.1 Regularizing with precomputed global embedding

In DREAMS, we first precompute the PCA positions $\widetilde{Y} \in \mathbb{R}^{n \times 2}$ as the reference embedding for global structure of the data. To combine the local structure preservation of t-SNE with the global structure

preservation of PCA, we augment the t-SNE loss function by a regularization term that penalizes embedding points Y deviating from their PCA positions $\widetilde{Y}$, yielding the loss

$$\mathcal{L}(Y) = (1-\lambda)\mathcal{L}_{t\text{-SNE}}(Y) + \frac{\lambda}{n}\|Y - \alpha\widetilde{Y}\|_F^2. \tag{2}$$

Since a PCA embedding scales linearly with the original data scale, while a t-SNE embedding does not, we rescale $\widetilde{Y}$ to match the scale of Y during each gradient-descent iteration by computing a scalar α

$$\alpha = \|Y\|_F / \|\widetilde{Y}\|_F. \tag{3}$$

This scaling encourages the reference embedding to match the current scale of the t-SNE embedding during optimization, making the global and local objectives more compatible. Note that α was treated as a constant in each gradient descent iteration. We discuss alternative scaling options in Appendix C.

The first term of Equation 2 enforces the preservation of local structure in the embedding by minimizing the t-SNE loss (Equation 1), while the regularization term ensures the preservation of global structure by encouraging the embedding to resemble the (scaled) PCA embedding $\widetilde{Y}$. This setup allows for local adjustments by the t-SNE loss, while the quadratic penalty prevents large deviations that would distort the global layout. The regularization strength λ controls the impact of the PCA embedding on the final embedding, thereby enabling a trade-off between local and global structure preservation. For $\lambda = 0$, DREAMS produces a standard t-SNE embedding since the loss term (Equation 2) reduces to the t-SNE objective. In the other limiting case of regularization strength $\lambda = 1$, the objective becomes the regularizer without the t-SNE loss whose optimum is a (scaled) PCA embedding. For intermediate $\lambda \in (0, 1)$ the objective is a weighted mean between t-SNE objective and the regularizer. Empirically, we found $\lambda = 0.1$ to be a suitable value for combining the individual strengths of global structure preservation of PCA with the local structure preservation of t-SNE without substantially compromising either aspect.

This framework is not limited to using the PCA embedding as $\widetilde{Y}$. Depending on the characteristics of the dataset, other methods with a good global structure preservation, such as MDS, can also be used as an effective choice for $\widetilde{Y}$. We will call the version of DREAMS that regularizes using the SQuadMDS embedding as DREAMS-MDS. By default, we use PCA instead of MDS because PCA is faster and is inherently interpretable due to its linearity.

Our implementation was based on the openTSNE library (Poličar et al., 2024) where we added the regularization term to the gradient descent optimization. We used default openTSNE hyperparameters and always initialized with the regularization embedding $\widetilde{Y}$. When using the PCA embedding as $\widetilde{Y}$, we normalized it by the standard deviation of PC1. When using the MDS embedding (DREAMS-MDS), we directly used the SQuadMDS output embedding, which performs some internal normalization and produces embeddings with standard deviations around 10 for all datasets.

The openTSNE library implements Barnes–Hut t-SNE (Yang et al., 2013; Van Der Maaten, 2014) and FIt-SNE (Linderman et al., 2019) approximations having runtime complexity $\mathcal{O}(n \log n)$ and $\mathcal{O}(n)$ respectively.

4.2 Linear decoding regularization

An alternative approach to using a precomputed PCA embedding is using a linear decoder. Equivalent to variance maximization, PCA can also be obtained by minimizing the reconstruction error

$$\widetilde{W} = \underset{W \in \mathbb{R}^{m \times d}}{\arg\min} \|X - XWW^T\|_F^2 \text{ subject to } W^T W = I_d. \tag{4}$$

Since the PCA embedding is given by $\widetilde{Y} = X\widetilde{W}$, the DREAMS loss including the decoding regularizer becomes

$$\mathcal{L}(Y, D) = (1-\lambda)\mathcal{L}_{t\text{-SNE}} + \lambda \left\|X - (YD^T + b)\right\|_F^2,$$

with $D \in \mathbb{R}^{m \times d}$ being a trainable linear decoder and $b \in \mathbb{R}^m$ a trainable bias term that is added row-wise and allows to handle uncentered embeddings. In this setup, by minimizing the reconstruction error, the decoder

Table 1: Datasets used in our experiments with a description of their local and global structure. For MNIST and Fashion MNIST, we only used the training set.

Name	**Description**	**Global structure**	**Local str.**	$\boldsymbol{n}$
Tasic et al.	scRNA-seq of mouse cortex	major cell classes	cell types	23 822
Macosko et al.	scRNA-seq of mouse retina	major cell classes	cell types	44 808
Kanton et al.	scRNA-seq of human brain	developmental trajectory	cell types	20 272
Wagner et al.	scRNA-seq of zebrafish embryos	developmental trajectory	cell types	63 530
Packer et al.	scRNA-seq of C. elegans	developmental trajectory	cell types	86 024
1000 Genomes	human whole-genome sequencing	continental ancestry	populations	3 450
Mammoth	3D Mammoth skeleton	overall body shape	bone structure	50 000
Satellite	satellite image crops	soil color	6 soil types	6435
FMNIST	images of fashion items	shoes/bags/garments	10 classes	60 000
MNIST	hand-written digits	none	digits 0–9	60 000
CIFAR10	vehicle and animal images	vehicle vs animals	10 classes	60 000

is responsible for the global structure preservation by pushing the embedding towards the PCA structure that has the minimal reconstruction error. If D were constrained to be orthogonal $D^T D = I_d$, the optimum of the regularization term would be $D = \widetilde{W}$ (Plaut, 2018; Nazari et al., 2023). Although we do not explicitly enforce orthogonality, we observed that the learned linear decoder D naturally tends to be approximately orthogonal.

We based our implementation on InfoNC-t-SNE (Damrich et al., 2023), a GPU-based contrastive learning approximation of t-SNE with the InfoNCE loss, implemented in PyTorch as CNE (contrastive neighbor embedding) package. This allowed us to add the decoding regularizer based on a linear PyTorch layer. We increased the number of negative samples to 500 to improve the local structure preservation and approximate t-SNE more closely. For the same reason, we ran the optimization for 750 epochs. The remaining hyperparameters were kept at default values. For the regularization term, we used a linear layer mapping the low-dimensional embedding to the original feature space. The weights were initialized using the first two principal components of the data (the bias term was initialized with zero). We will refer to this version as DREAMS-CNE-Decoder.

For comparison, we also implemented a version of DREAMS using the CNE backend with precomputed PCA regularization as in Section 4.1. We will refer to this version as DREAMS-CNE. Here the gradient with respect to Y was computed using autodifferentiation, including the $\|Y\|_F$ contribution to α.

5 Experimental setup

5.1 Datasets and metrics

To validate our method experimentally, we used eleven real-world datasets, all but one containing both prominent local and global structures (Table 1). We measured the embedding quality using two established metrics quantifying local and global structure preservation (Kobak and Berens, 2019):

KNN The k-nearest neighbor recall (KNN) is the fraction of k-nearest neighbors in the high-dimensional data that are preserved as k-nearest neighbors in the low-dimensional embedding. We used $k = 10$ throughout all experiments (for results with different choices of k see Figure S5). The final metric is given as the average across all n data points. KNN quantifies the preservation of local structure in the embedding.

CPD The correlation of pairwise distances (CPD) is the Spearman correlation between the pairwise distances in the high-dimensional space and in the embedding. We computed pairwise distances among 1 000 randomly chosen data points. CPD quantifies the preservation of the global structure in the embedding.

These two metrics rely solely on the high-dimensional data X and its corresponding embedding Y and do not make use of any metadata listed in Table 1.

We also evaluated an aggregated local-global score s. For each dataset, we normalized both metrics based on the minimum and the maximum values observed across all methods. Let $\mathrm{KNN}_{\mathrm{min}}$ and $\mathrm{CPD}_{\mathrm{min}}$ denote the lowest (worst) KNN and CPD scores across all methods for a given dataset, and $\mathrm{KNN}_{\mathrm{max}}$ and $\mathrm{CPD}_{\mathrm{max}}$ denote the highest (best) scores. Given an embedding with specific KNN and CPD values, we define the aggregated local-global score as

$$s = \frac{1}{2}\left(\frac{\mathrm{KNN} - \mathrm{KNN}_{\mathrm{min}}}{\mathrm{KNN}_{\mathrm{max}} - \mathrm{KNN}_{\mathrm{min}}} + \frac{\mathrm{CPD} - \mathrm{CPD}_{\mathrm{min}}}{\mathrm{CPD}_{\mathrm{max}} - \mathrm{CPD}_{\mathrm{min}}}\right). \tag{5}$$

This score ranges from 0 (embedding has the worst local and the worst global scores) to 1 (embedding has the best local and the best global scores), and allows direct comparison of embedding methods regarding their combined local and global structure preservation. Note that it only produces a relative score as it depends on the considered competitors. For an intuitive understanding of the local-global score see Figure S4.

5.2 Comparison methods

We validated DREAMS against several baseline and hybrid methods (always using the default hyperparameter settings):

- t-SNE (van der Maaten and Hinton, 2008) using the openTSNE implementation (Poličar et al., 2024) with the same initialization as in DREAMS (PCA normalized by the standard deviation of PC1), and UMAP (McInnes et al., 2018) as baselines for local structure preservation;
- PCA and MDS using the SQuadMDS implementation (Lambert et al., 2022) as baselines for global structure preservation;
- TriMap (Amid and Warmuth, 2019), PacMAP (Wang et al., 2023), and PHATE (Moon et al., 2019) as a methods that strive to preserve both local and global structure;
- and hybrid approaches SQuadMDS-hybrid (Lambert et al., 2022) and StarMAP (Watanabe et al., 2025), which, like DREAMS, mix the local structure preservation of neighbor embeddings with global methods.

We always report means and uncertainties (often barely perceptible) across four random seeds. All experiments were conducted on a single Intel Xeon Gold 6226R CPU 2.90 GHz (16 cores, 32 threads), an NVIDIA RTX A6000 GPU (48 GB VRAM, CUDA 12.7), and 377 GB system RAM, running on a Linux environment. Only experiments including DREAMS-CNE or DREAMS-CNE-Decoder utilized the GPU. Without parallelization, the runtime of all experiments was about a week. For a runtime analysis of DREAMS and its competitors, see Figure S3.

6 Results

6.1 DREAMS successfully combines the strengths of t-SNE and PCA

We first illustrate DREAMS using the Tasic et al. dataset. When adjusting the regularization strength λ, DREAMS generates a continuum of embeddings between the two extremes of the locally focused t-SNE embedding and the globally focused PCA embedding (Figure 2a). For small λ values, the resulting embedding resembled the t-SNE embedding, effectively capturing the local data structure and highlighting fine-grained clusters and cell types. For larger λ values, the embedding progressively shifted towards the PCA embedding, emphasizing higher-level groupings, such as broad cell classes (inhibitory/excitatory neurons and non-neuronal cells). At intermediate regularization strengths, DREAMS integrated both local and global structures without visibly compromising either aspect of the data. Competing methods often missed much of the global structure (Figure 2b, c) or showed less local structure (Figure 2c–e).

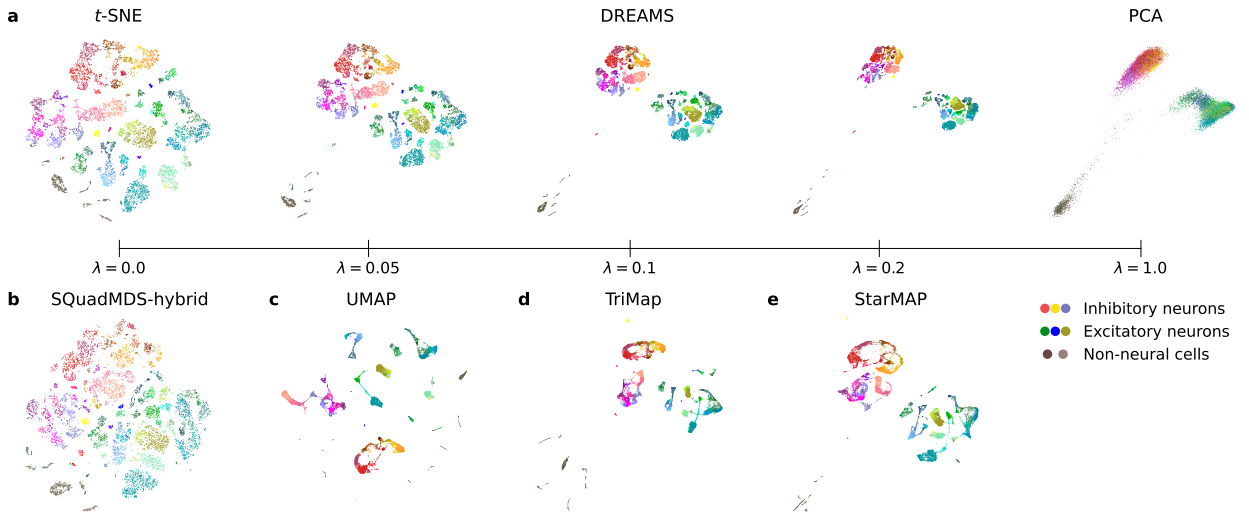

Figure 2: Embeddings of the Tasic et al. dataset. **a** Spectrum of DREAMS embeddings for different values of λ. **b** Embeddings obtained by some of the competing methods. For all embeddings, see Figure S6.

The quantitative metrics corroborated DREAMS ability to maintain both local and global structure (Figure 3). On all datasets but Mammoth, t-SNE achieved the highest KNN value, providing the best locally structured embedding. In contrast, PCA and MDS maintained global structure best, as reflected in their CPD values being the highest. For nearly all regularization parameters $\lambda \in [0, 1]$ DREAMS yielded embeddings with better local or global structure preservation than its competitors. On most datasets, DREAMS with its default regularization strength ($\lambda = 0.1$) simultaneously achieved KNN close to t-SNE's and CPD close to PCA's. Across all datasets, DREAMS preserved the local structure much better than StarMAP, which also combines neighbor embeddings with PCA. This is likely because DREAMS relies on t-SNE, which preserves local structure better than UMAP, which is used in StarMAP.

UMAP generally performed poorly in our metrics, often preserving not only the local but also the global structure worse than t-SNE, as measured by the CPD metric. This is likely due to different default initializations of openTSNE and UMAP (PCA and Laplacian Eigenmaps, respectively). In contrast, TriMap often performed similarly well to StarMap, but still fell short compared to DREAMS in terms of local structure preservation. PHATE and PacMAP yielded worse CPD and worse KNN scores compared to DREAMS on all datasets.

On the MNIST dataset DREAMS was not able to maintain high global and local structure at the same time, likely because this dataset does not have a prominent global structure in the first place (CPD values were comparatively low for all methods including PCA and MDS). Similarly, on the pixel-valued CIFAR10 dataset, DREAMS incurred a clear trade-off between local and global structure. On this challenging dataset all methods severely struggled (Figure S16). Nevertheless, even in these two cases, DREAMS was on par or outperformed most other methods (Figure 3g).

Using our aggregated local-global score, we could directly compare DREAMS to other methods along a single dimension (Table 2). The highest local-global score on every dataset was achieved either by DREAMS or by DREAMS-MDS, depending on whether PCA or MDS was capturing global structure more effectively in terms of the CPD metric. Following DREAMS, SQuadMDS-hybrid was consistently the next best method. It achieved scores comparable to DREAMS on 3 datasets, but on all remaining datasets, its performance measured by the local-global score was at least 6% lower than the best performing DREAMS variant. On the dataset where DREAMS achieve a good balance between local and global performance (all but MNIST and CIFAR10) all remaining other methods had scores at least 9% lower than the best performing DREAMS variant.

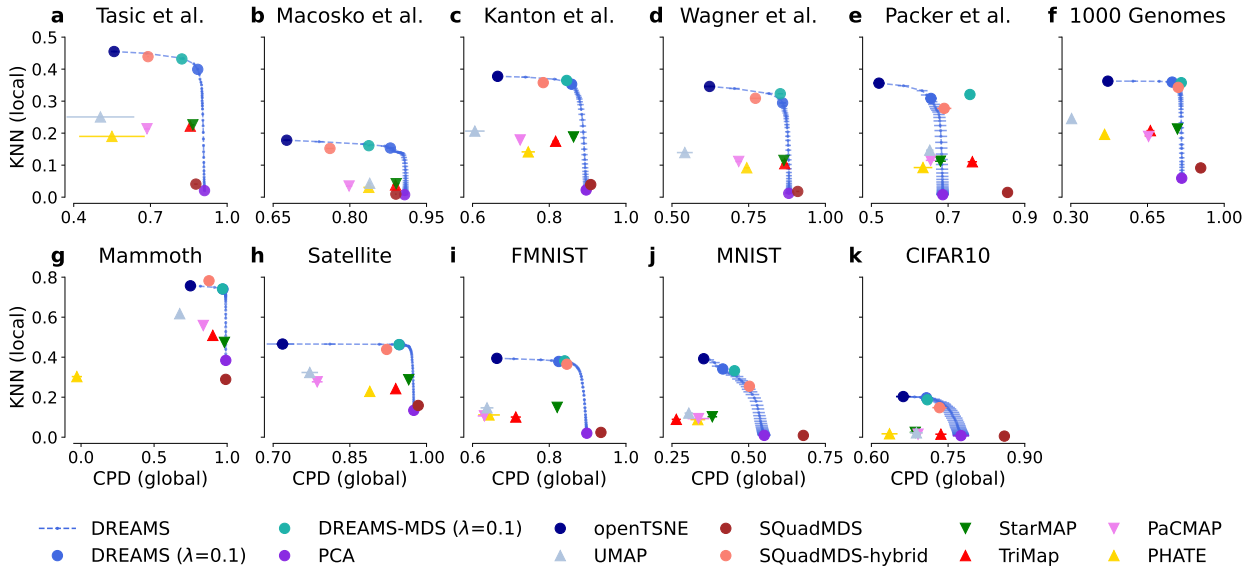

Figure 3: Quantitative evaluation of local and global structure preservation of different methods across multiple datasets (Table 1). Spearman correlation of pairwise distances (CPD, global metric) is plotted against kNN recall (KNN, local metric). For improved visual clarity different markers were used.

6.2 DREAMS provides the best local-global spectrum

Next we compared the local-global embedding spectrum of DREAMS to the local-global spectra of existing methods and variants of DREAMS.

In SQuadMDS-hybrid, the spectrum of embeddings is obtained by specifying the learning rates of t-SNE and MDS. For StarMAP, varying the regularization strength allows trading off local and global structure. Furthermore, increasing the exaggeration parameter in openTSNE can emphasize global structure preservation and also yields a local-global continuum of embeddings (Böhm et al., 2022).

We observed that these spectra offered noticeably worse trade-offs than DREAMS, as illustrated on the Tasic et al. dataset in Figure 4a, where PCA produces the best global layout. Similarly, DREAMS-MDS achieves

Table 2: Aggregated local-global score. For each dataset, the methods within 0.05 of the highest score are highlighted in bold. The order of the datasets is as in Table 1.

	Tas	Mac	Kan	Wag	Pac	1kG	Mam	Sat	FMN	MNI	C10
DREAMS	**0.91**	**0.87**	**0.88**	**0.86**	0.62	**0.89**	**0.95**	**0.93**	**0.80**	**0.62**	**0.64**
DREAMS-MDS	**0.87**	0.80	**0.90**	**0.89**	**0.81**	**0.92**	**0.95**	**0.93**	**0.83**	**0.67**	**0.62**
SQuadMDS-hybrid	0.71	0.61	0.77	0.76	0.63	**0.88**	**0.94**	0.84	**0.81**	0.61	0.58
StarMAP	0.68	0.56	0.66	0.59	0.38	0.66	0.68	0.70	0.49	0.26	0.16
PHATE	0.25	0.42	0.40	0.39	0.28	0.35	0.01	0.46	0.14	0.19	0.03
PaCMAP	0.45	0.35	0.42	0.39	0.35	0.51	0.70	0.34	0.12	0.20	0.15
TriMap	0.66	0.55	0.56	0.58	0.51	0.55	0.68	0.58	0.24	0.10	0.25
UMAP	0.26	0.46	0.26	0.19	0.39	0.31	0.68	0.39	0.18	0.19	0.16
t-SNE	0.60	0.50	0.60	0.63	0.50	0.73	0.86	0.50	0.55	0.61	0.56
PCA	0.50	0.50	0.48	0.46	0.24	0.43	0.60	0.48	0.44	0.35	0.32
MDS	0.48	0.47	0.52	0.51	0.51	0.55	0.50	0.54	0.51	0.50	0.50

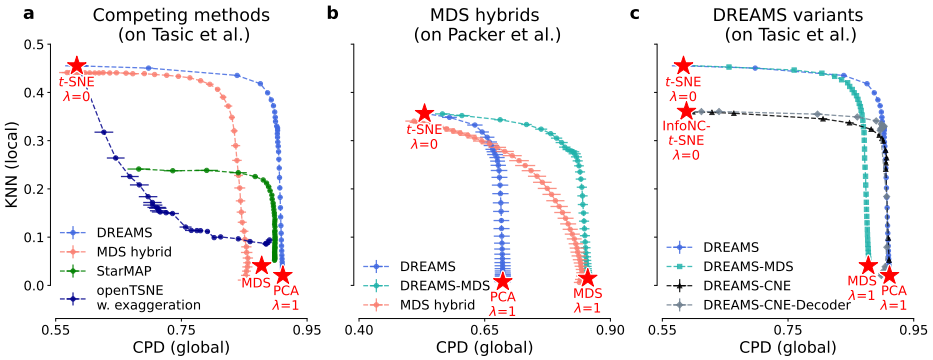

Figure 4: Trade-offs between local and global structure preservation in different methods. Spearman correlation of pairwise distances is plotted against kNN recall. Panels **a** and **c** show results on the Tasic et al. dataset, while panel **b** is based on the Packer et al. dataset. **a**: Performance of DREAMS compared with other local-global spectra. **b**: Comparison of DREAMS-MDS and SQuadMDS-hybrid. **c**: Performance of different DREAMS variants.

a better trade-off than SQuadMDS-hybrid, as demonstrated on the Packer et al. dataset (Figure 4b), where MDS produces the best global layout.

Moreover, while DREAMS includes standard t-SNE and PCA/MDS as its corner cases for $\lambda = 0$ and $\lambda = 1$ (marked with stars in Figure 4), neither SQuadMDS-hybrid nor StarMAP could reach MDS and PCA, respectively, in their most global setting. Additionally, SQuadMDS-hybrid underperformed compared to t-SNE in its most local configuration (Figure 4a,b). This outcome is expected for StarMAP, as its objective continues to blend aspects of UMAP and PCA, even at its highest regularization strength. In the case of SQuadMDS-hybrid, the reason is likely the normalization of the t-SNE and MDS gradients before combining them.

Switching DREAMS' neighbor-embedding backend from openTSNE to contrastive neighbor embeddings (CNE, Damrich et al. 2023) with the InfoNCE loss decreased the local structure preservation, directly proportionally to the difference in local structure preservation between t-SNE and its InfoNCE version InfoNC-t-SNE (Figure 4c). Using the CNE backend, we compared regularization using a precomputed PCA embedding (DREAMS-CNE) with linear decoding regularization (DREAMS-CNE-Decoder), and observed only marginal improvements with the decoder approach (Figure S1). The MNIST dataset was the only one where the decoder approach performed much better in terms of our metrics, but this did not translate into visible improvements of the embedding structure. Although the decoder could reconstruct the PCA embedding and enhance global structure, it introduces additional randomness and computational complexity. Moreover, with a precomputed global embedding, we are more flexible to adjust the global layout e.g. by switching from PCA to MDS. For these reasons and especially due to the better local structure of openTSNE than InfoNC-t-SNE, we prefer the simple regularization using a precomputed embedding as in the openTSNE-based DREAMS variants.

7 Discussion

In this work, we introduced DREAMS, a dimensionality reduction method that adds a regularization term to the t-SNE objective. This regularization term penalizes embedding points that deviate from their corresponding PCA positions and thereby encourages global structure preservation throughout the optimization process. Our approach addresses a critical shortcoming in conventional dimensionality reduction techniques, which often prioritize one structural scale over the other. Through this simple yet effective regularization term and a tunable hyperparameter λ, DREAMS allows for a continuous spectrum of embeddings that transition smoothly from the locally faithful structure of t-SNE to the globally coherent and interpretable structure of PCA. Furthermore, with its default regularization strength ($\lambda = 0.1$), DREAMS provides an embedding that successfully balances local and global structure preservation, outperforming competing methods.

Across eleven real-world datasets, DREAMS or DREAMS-MDS with default $\lambda = 0.1$ consistently achieved the best performance in terms of the local-global score. This highlights its robustness and wide applicability, especially to hierarchical datasets with multiple inherent structure scales. While multiscale structure is common in real-world datasets, DREAMS is less useful in datasets without it, such as the MNIST dataset, as there is less global structure to preserve. In particular, we do not have theoretical performance guarantees ensuring that DREAMS will balance local and global structure well. Moreover, DREAMS introduces an additional hyperparameter, the regularization strength λ, whose optimal value can depend on the specific dataset and the intended use. Consequently, different datasets may require tuning λ to achieve the optimal balance between local and global structure preservation. That said, we found that $\lambda = 0.1$ worked well across the datasets.

Because the regularization enforces alignment with a predefined structure, any biases or limitations in the PCA embedding would propagate into the final embedding. As demonstrated in cases where the MDS embedding captures global structure more effectively than PCA, sometimes it can be beneficial to regularize towards the MDS embedding, as in DREAMS-MDS. Thanks to its flexible and simple design, DREAMS accommodates such substitutions, making it adaptable to the specific characteristics of different datasets.

Our alternative implementation DREAMS-CNE-Decoder performed worse than the default DREAMS due to the lower local quality of sampling-based InfoNC-t-SNE. Therefore we prefer our openTSNE-based implementation, even though the PyTorch implementation may be preferable in some use cases.

In conclusion, DREAMS successfully combines the local structure preservation strength of t-SNE with the global structure of PCA. This makes DREAMS' visualizations of high-dimensional data more faithful and interpretable, particularly for datasets with hierarchical structure.

References

Ehsan Amid and Manfred K Warmuth. TriMap: Large-scale dimensionality reduction using triplets. *arXiv preprint arXiv:1910.00204*, 2019.

Mikhail Belkin and Partha Niyogi. Laplacian Eigenmaps for dimensionality reduction and data representation. *Neural Computation*, 15(6):1373–1396, 2003.

Jan Niklas Böhm, Philipp Berens, and Dmitry Kobak. Attraction-repulsion spectrum in neighbor embeddings. *Journal of Machine Learning Research*, 23(95):1–32, 2022.

Sebastian Damrich, Niklas Böhm, Fred A Hamprecht, and Dmitry Kobak. From t-SNE to UMAP with contrastive learning, 2023.

Cyril De Bodt, Dounia Mulders, Michel Verleysen, and John Aldo Lee. Fast multiscale neighbor embedding. *IEEE Transactions on Neural Networks and Learning Systems*, 33(4):1546–1560, 2020.

Alex Diaz-Papkovich, Luke Anderson-Trocmé, Chief Ben-Eghan, and Simon Gravel. UMAP reveals cryptic population structure and phenotype heterogeneity in large genomic cohorts. *PLoS Genetics*, 15(11): e1008432, 2019.

Alex Diaz-Papkovich, Shadi Zabad, Chief Ben-Eghan, Luke Anderson-Trocmé, Georgette Femerling, Vikram Nathan, Jenisha Patel, and Simon Gravel. Topological stratification of continuous genetic variation in large biobanks. *bioRxiv*, 2023.

Jiarui Ding, Anne Condon, and Sohrab P Shah. Interpretable dimensionality reduction of single cell transcriptome data with deep generative models. *Nature Communications*, 9(1):2002, 2018.

Andres F Duque, Sacha Morin, Guy Wolf, and Kevin R Moon. Geometry Regularized Autoencoders. *IEEE Transactions on Pattern Analysis and Machine Intelligence*, 45(6):7381–7394, 2022.

Mateus Espadoto, Rafael M Martins, Andreas Kerren, Nina ST Hirata, and Alexandru C Telea. Toward a quantitative survey of dimension reduction techniques. *IEEE Transactions on Visualization and Computer Graphics*, 27(3):2153–2173, 2019.

Colin Goodall. Procrustes methods in the statistical analysis of shape. *Journal of the Royal Statistical Society: Series B (Methodological)*, 53(2):285–321, 1991.

John C Gower. Generalized procrustes analysis. *Psychometrika*, 40(1):33–51, 1975.

Jacob M Graving and Iain D Couzin. VAE-SNE: a deep generative model for simultaneous dimensionality reduction and clustering. *BioRxiv*, pages 2020–07, 2020.

Harold Hotelling. Analysis of a complex of statistical variables into principal components. *Journal of Educational Psychology*, 24(6):417, 1933.

Haiyang Huang, Yingfan Wang, Cynthia Rudin, and Edward P Browne. Towards a comprehensive evaluation of dimension reduction methods for transcriptomic data visualization. *Communications Biology*, 5(1):719, 2022.

Sabina Kanton, Michael James Boyle, Zhisong He, Malgorzata Santel, Anne Weigert, Fátima Sanchís-Calleja, Patricia Guijarro, Leila Sidow, Jonas Simon Fleck, Dingding Han, et al. Organoid single-cell genomic atlas uncovers human-specific features of brain development. *Nature*, 574(7778):418–422, 2019.

Dmitry Kobak and Philipp Berens. The art of using t-SNE for single-cell transcriptomics. *Nature Communications*, 10(1):5416, 2019.

Dmitry Kobak and George C Linderman. Initialization is critical for preserving global data structure in both t-SNE and UMAP. *Nature Biotechnology*, 39(2):156–157, 2021.

Alex Krizhevsky, Geoffrey Hinton, et al. Learning multiple layers of features from tiny images. 2009.

Joseph B Kruskal. Multidimensional scaling by optimizing goodness of fit to a nonmetric hypothesis. *Psychometrika*, 29(1):1–27, 1964.

Pierre Lambert, Cyril De Bodt, Michel Verleysen, and John A Lee. SQuadMDS: A lean stochastic quartet MDS improving global structure preservation in neighbor embedding like t-SNE and UMAP. *Neurocomputing*, 503:17–27, 2022.

Y. Lecun, L. Bottou, Y. Bengio, and P. Haffner. Gradient-based learning applied to document recognition. *Proceedings of the IEEE*, 86(11):2278–2324, 1998. doi: 10.1109/5.726791.

John A Lee, Diego H Peluffo-Ordóñez, and Michel Verleysen. Multi-scale similarities in stochastic neighbour embedding: Reducing dimensionality while preserving both local and global structure. *Neurocomputing*, 169:246–261, 2015.

George C Linderman, Manas Rachh, Jeremy G Hoskins, Stefan Steinerberger, and Yuval Kluger. Fast interpolation-based t-SNE for improved visualization of single-cell RNA-seq data. *Nature Methods*, 16(3): 243–245, 2019.

Evan Z Macosko, Anindita Basu, Rahul Satija, James Nemesh, Karthik Shekhar, Melissa Goldman, Itay Tirosh, Allison R Bialas, Nolan Kamitaki, Emily M Martersteck, et al. Highly parallel genome-wide expression profiling of individual cells using nanoliter droplets. *Cell*, 161(5):1202–1214, 2015.

Leland McInnes, John Healy, and James Melville. UMAP: Uniform manifold approximation and projection for dimension reduction. *arXiv preprint arXiv:1802.03426*, 2018.

Jacob Miller, Vahan Huroyan, and Stephen Kobourov. Balancing between the local and global structures (LGS) in graph embedding, 2023.

Kevin R Moon, David Van Dijk, Zheng Wang, Scott Gigante, Daniel B Burkhardt, William S Chen, Kristina Yim, Antonia van den Elzen, Matthew J Hirn, Ronald R Coifman, et al. Visualizing structure and transitions in high-dimensional biological data. *Nature Biotechnology*, 37(12):1482–1492, 2019.

Philipp Nazari, Sebastian Damrich, and Fred A Hamprecht. Geometric autoencoders: what you see is what you decode. In *Proceedings of the 40th International Conference on Machine Learning*, pages 25834–25857, 2023.

Max Noichl. Examples for umap-dimensionality reduction using 3D models of prehistoric animals. `https://doi.org/10.5281/zenodo.17290165`, 2025. Version 0.0.1 [Dataset]. Zenodo.

David Novak, Cyril de Bodt, Pierre Lambert, John A Lee, Sofie Van Gassen, and Yvan Saeys. Interpretable models for scRNA-seq data embedding with multi-scale structure preservation. *bioRxiv*, pages 2023–11, 2023.

Jonathan S Packer, Qin Zhu, Chau Huynh, Priya Sivaramakrishnan, Elicia Preston, Hannah Dueck, Derek Stefanik, Kai Tan, Cole Trapnell, Junhyong Kim, et al. A lineage-resolved molecular atlas of C. elegans embryogenesis at single-cell resolution. *Science*, 365(6459):eaax1971, 2019.

Karl Pearson. Liii. On lines and planes of closest fit to systems of points in space. *The London, Edinburgh, and Dublin Philosophical Magazine and Journal of Science*, 2(11):559–572, 1901.

Elad Plaut. From principal subspaces to principal components with linear autoencoders. *arXiv preprint arXiv:1804.10253*, 2018.

Pavlin G Poličar, Martin Stražar, and Blaž Zupan. openTSNE: a modular Python library for t-SNE dimensionality reduction and embedding. *Journal of Statistical Software*, 109:1–30, 2024.

Smithsonian Institution. Mammuthus primigenius (Blumbach) [3D model]. `https://3d.si.edu/object/3d/mammuthus-primigenius-blumbach:341c96cd-f967-4540-8ed1-d3fc56d31f12`, 2020.

Ashwin Srinivasan. Statlog (Landsat Satellite). UCI Machine Learning Repository, 1993. DOI: https://doi.org/10.24432/C55887.

Benjamin Szubert, Jennifer E Cole, Claudia Monaco, and Ignat Drozdov. Structure-preserving visualisation of high dimensional single-cell datasets. *Scientific Reports*, 9(1):8914, 2019.

Bosiljka Tasic, Zizhen Yao, Lucas T Graybuck, Kimberly A Smith, Thuc Nghi Nguyen, Darren Bertagnolli, Jeff Goldy, Emma Garren, Michael N Economo, Sarada Viswanathan, et al. Shared and distinct transcriptomic cell types across neocortical areas. *Nature*, 563(7729):72–78, 2018.

The 1000 Genomes Project Consortium. A global reference for human genetic variation. *Nature*, 526(7571):68–74, 2015.

Laurens Van Der Maaten. Accelerating t-SNE using tree-based algorithms. *The Journal of Machine Learning Research*, 15(1):3221–3245, 2014.

Laurens van der Maaten and Geoffrey Hinton. Visualizing data using t-SNE. *Journal of Machine Learning Research*, 9(Nov):2579–2605, 2008.

Daniel E Wagner, Caleb Weinreb, Zach M Collins, James A Briggs, Sean G Megason, and Allon M Klein. Single-cell mapping of gene expression landscapes and lineage in the zebrafish embryo. *Science*, 360(6392):981–987, 2018.

Kaiwen Wang, Yuqiu Yang, Fangjiang Wu, Bing Song, Xinlei Wang, and Tao Wang. Comparative analysis of dimension reduction methods for cytometry by time-of-flight data. *Nature Communications*, 14(1):1836, 2023.

Yingfan Wang, Haiyang Huang, Cynthia Rudin, and Yaron Shaposhnik. Understanding how dimension reduction tools work: an empirical approach to deciphering t-SNE, UMAP, TriMAP, and PaCMAP for data visualization. *Journal of Machine Learning Research*, 22(201):1–73, 2021.

Koshi Watanabe, Keisuke Maeda, Takahiro Ogawa, and Miki Haseyama. StarMAP: Global neighbor embedding for faithful data visualization. *arXiv preprint arXiv:2502.03776*, 2025.

Han Xiao, Kashif Rasul, and Roland Vollgraf. Fashion-mnist: a novel image dataset for benchmarking machine learning algorithms. *arXiv preprint arXiv:1708.07747*, 2017.

Zhirong Yang, Jaakko Peltonen, and Samuel Kaski. Scalable optimization of neighbor embedding for visualization. In Sanjoy Dasgupta and David McAllester, editors, *Proceedings of the 30th International Conference on Machine Learning*, volume 28 of *Proceedings of Machine Learning Research*. PMLR, 2013.

Appendix

A Datasets

All scRNA-seq datasets (except Packer et al.) were preprocessed as in Böhm et al. (2022) and Kobak and Berens (2019). After selecting the 1000 (3000 for Macosko et al.) most variable genes, we normalized the library sizes to the median library size in the dataset, log-transformed the normalized values with $\log_2(x+1)$, and finally reduced the dimensionality to 50 via PCA. The Packer et al. dataset was already preprocessed to 100 principal components of which we used the first 50. The original data was downloaded following links in the original publications.

The raw 1000 Genomes Project data (The 1000 Genomes Project Consortium, 2015) is available at `https://ftp.1000genomes.ebi.ac.uk`. This dataset contains 3 450 human genotypes. We got the preprocessed data from (Diaz-Papkovich et al., 2019) and (Diaz-Papkovich et al., 2023); this is in an integer-valued data matrix with 53 999 features, containing values 0, 1, and 2, representing the number of alleles differing from a reference genome. We used PCA to reduce the number of features to 50.

We used 50,000 unprocessed random samples of the Mammoth dataset (Smithsonian Institution, 2020; Noichl, 2025) and likewise used the unprocessed Landsat Satellite (Srinivasan, 1993) dataset. For the Mammoth dataset, cluster labels used solely for coloring the visualizations were obtained by applying Agglomerative Clustering with 11 classes to the original data.

For the MNIST (Lecun et al., 1998), Fashion MNIST (Xiao et al., 2017) (both downloaded using the torchvision API) and CIFAR10 (Krizhevsky et al., 2009) datasets, we used the first 50 principal components. For Fashion MNIST, we additionally rescaled the original data to the interval $[0, 1]$ before computing the first 50 principal components.

B DREAMS-CNE and DREAMS-CNE-Decoder

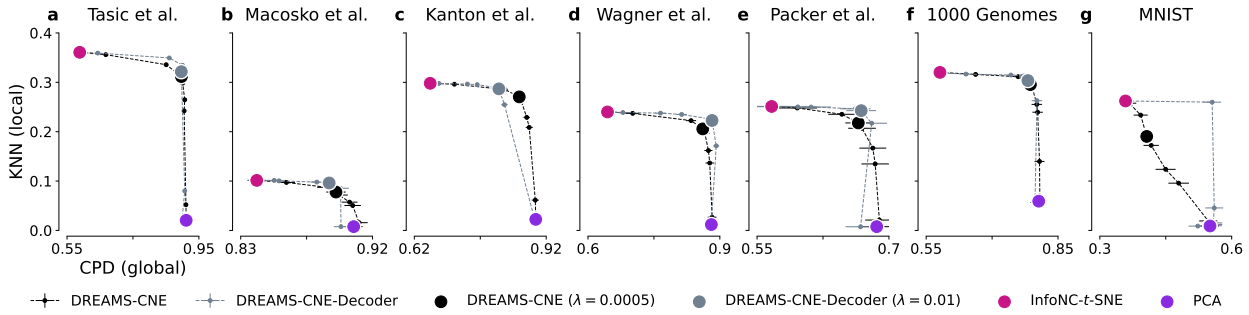

Figure S1: Spearman correlation of pairwise distances (CPD, global metric) is plotted against kNN recall (local metric). The figure shows the spectrum of DREAMS-CNE, using a regularizer with precomputed PCA embedding, and DREAMS-CNE-Decoder, using a regularizer with a linear decoder, across all seven datasets. The bigger scatter points display DREAMS-CNE and DREAMS-CNE-Decoder with their respective default regularization strengths (which achieved the highest average local-global score across all data sets) and reference methods. Here, InfoNC-t-SNE is used as the t-SNE backbone and corresponds to the regularization strength of $\lambda = 0$ while PCA corresponds to the maximal regularization strength of $\lambda = 1$. In panel g (MNIST) the scatter points of PCA and DREAMS-CNE-Decoder lie exactly on top of each other.

C Scaling of the global embedding in the DREAMS loss function

In the regularization term

$$\mathcal{R}(Y) = \frac{1}{n}\|Y - \alpha\widetilde{Y}\|_F^2, \tag{6}$$

the scaling parameter α is used to match the scale of the global reference embedding $\widetilde{Y}$ with that of Y. We considered two scaling strategies:

$$\alpha_n = \frac{\|Y\|_F}{\|\widetilde{Y}\|_F}, \quad \alpha_p = \frac{\langle Y, \widetilde{Y}\rangle_F}{\|\widetilde{Y}\|_F^2}. \tag{7}$$

By the Cauchy–Schwarz inequality, $\alpha_n \geq \alpha_p$, with equality iff Y is a positive rescaling of $\widetilde{Y}$. The first option, α_n, rescales $\widetilde{Y}$ to match the scale of Y, preventing the regularization term from imposing an artificial scale onto the scale-sensitive t-SNE embedding. The second option, α_p, is the α that minimizes the regularization term $\mathcal{R}(Y)$ for a given Y and $\widetilde{Y}$ and is inspired by Procrustes analysis (Goodall, 1991; Gower, 1975).

In preliminary experiments we found that α_p performed slightly worse than α_n on the Tasic et al. dataset, leading to lower structure preservation as measured by both performance metrics (KNN and CPD, Table S1). While the regularization term was, by construction, smaller with α_p, the KL divergence was slightly higher and the scale of the final embedding was further from t-SNE' than with α_n (Figure S2). Consequently, we chose to use the scaling with α_n and conducted all subsequent experiments with this scaling method. Importantly, both scaling strategies worked much better than not using scaling at all and fixing $\alpha = 1$ (Figure S2, Table S1).

Treating α as a constant during optimization yields the gradient

$$\nabla_Y \mathcal{R}(Y) = \frac{2}{n}\left(Y - \alpha\widetilde{Y}\right), \tag{8}$$

which pulls Y towards the scaled global reference embedding $\alpha\widetilde{Y}$. Using α_n scaling and allowing the gradients to propagate through α, yields the gradient

$$\nabla_Y \mathcal{R}(Y) = \frac{2}{n}\left(Y - \alpha\tilde{Y}\right) - \frac{2}{n}\left(\frac{\langle Y, \tilde{Y}\rangle}{\|Y\|_F\|\tilde{Y}\|_F} - 1\right)Y, \tag{9}$$

with an additional second term that corresponds to a shrinkage of Y towards the origin, since $\frac{\langle Y,\tilde{Y}\rangle}{\|Y\|_F\|\tilde{Y}\|_F} \leq 1$. As mentioned above, since the t-SNE loss is scale-sensitive, we do not want the regularizer to have a bearing on the scale of Y. Nevertheless, in the CNE variant of DREAMS, we did propagate gradient through α and still obtained a good trade-off between the InfoNC-t-SNE and PCA performance (Figure 4). We also verified that treating α as a constant in the CNE version did not produce any noticeable difference in performance.

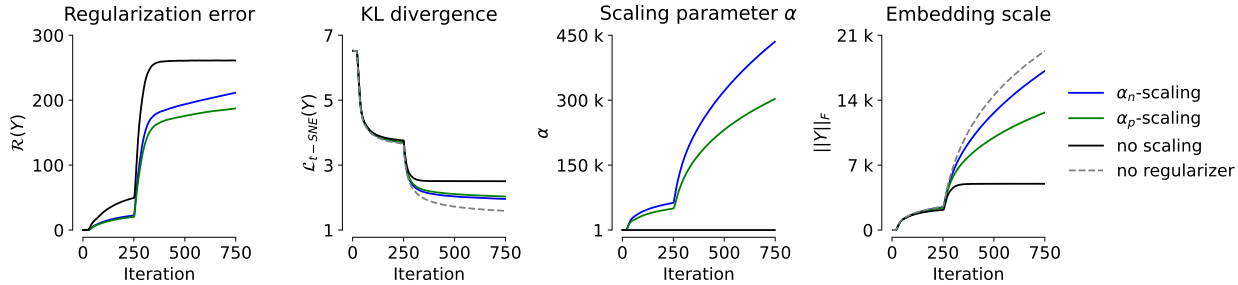

Figure S2: Regularization error, KL divergence, scaling parameter α and embedding scale of DREAMS during optimization using different or no scaling methods. Results are reported as the mean over four random seeds on the Tasic et al. dataset.

Table S1: Comparison of DREAMS performance across various alignment approaches for matching $\widetilde{Y}$ and Y on the Tasic et al. dataset. We compare default DREAMS with DREAMS using a lower scaling factor α_p, additionally translationally aligned the global reference $\tilde{Y}$ to Y (treating the shift as constant), and full Procrustes analysis, which also contains a rotational alignment. The smaller scaling with α_p was detrimental, while translational and rotational alignment had no effect as the t-SNE loss is invariant to them.

Metric	DREAMS (α_n)	α_p	α_p + translation	full Procrustes	no scaling
KNN	**0.40**	0.39	0.39	0.39	0.32
CPD	**0.89**	0.86	0.86	0.86	0.53

D Runtime analysis

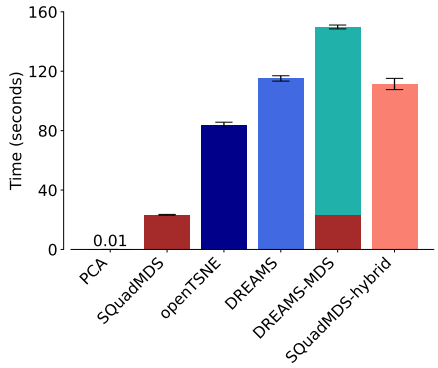

Figure S3: Runtime comparison. The bars indicate the mean runtime and standard deviation across four random seed on the Tasic et al. dataset. For DREAMS and DREAMS-MDS, the reported times also include the runtime of the respective global reference embeddings (PCA and MDS).

E Intuition of local-global score

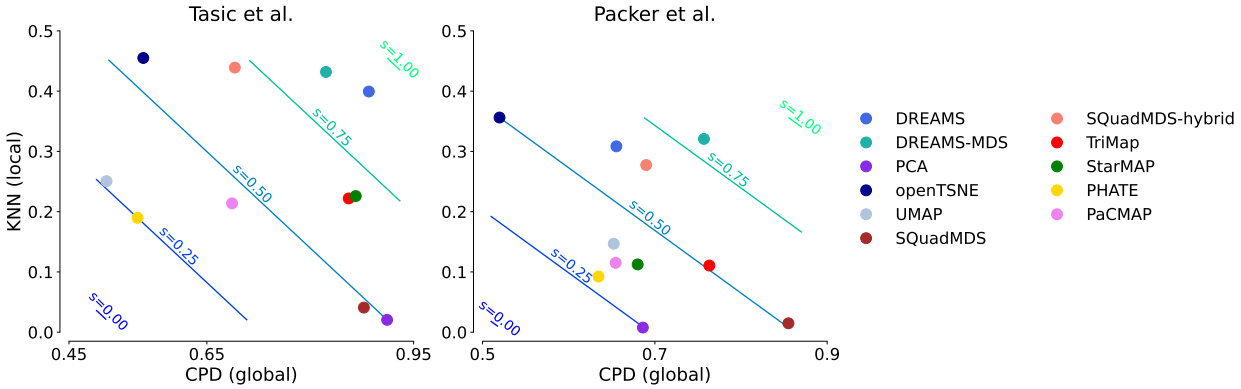

Figure S4: Spearman correlation of pairwise distances (CPD, global metric) is plotted against kNN recall (KNN, local metric) for different methods with marked local-global score spectrum. The figure shows the structure preservation results on the Tasic et al. and Packer et al. dataset.

F Sensitivity of kNN recall to choice of k

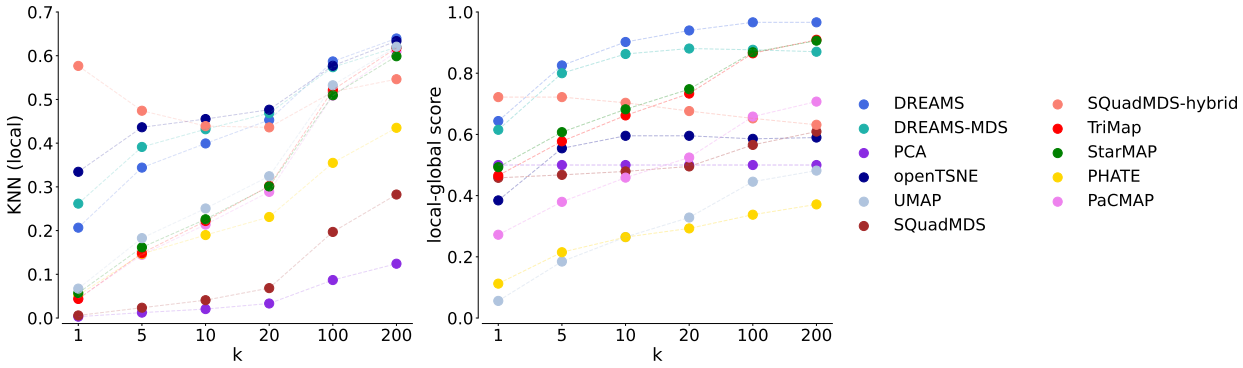

Figure S5: Local structure preservation metric and combined local-global score for different choices of k. Displayed are the results on the Tasic et al. dataset. Save for SquadMDS-hybrid, the ranking of methods in terms of KNN recall is insensitive to the exact value of k.

F.1 Visualizations of all datasets

See next pages.

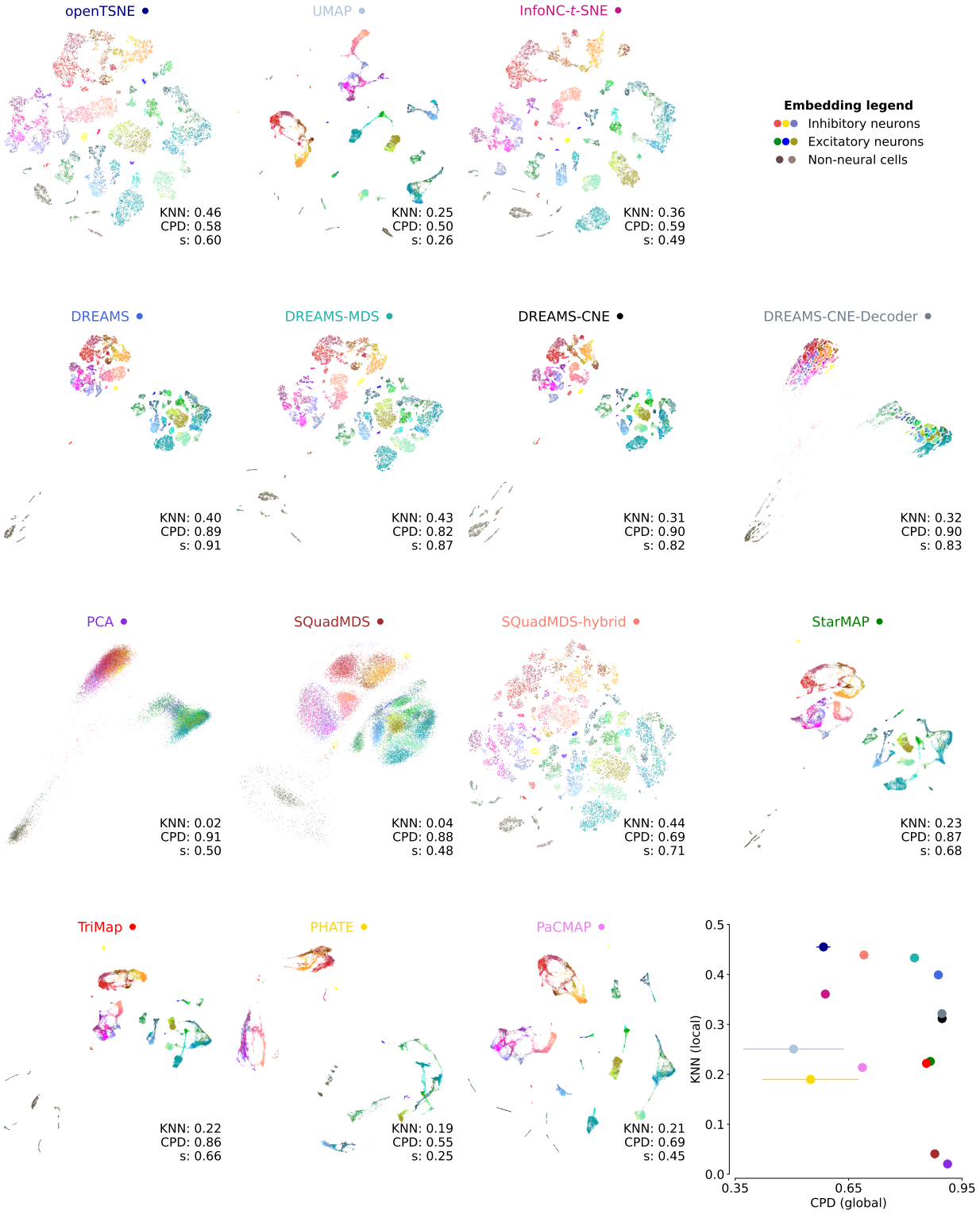

Figure S6: Visualizations of the Tasic et al. dataset with all considered methods.

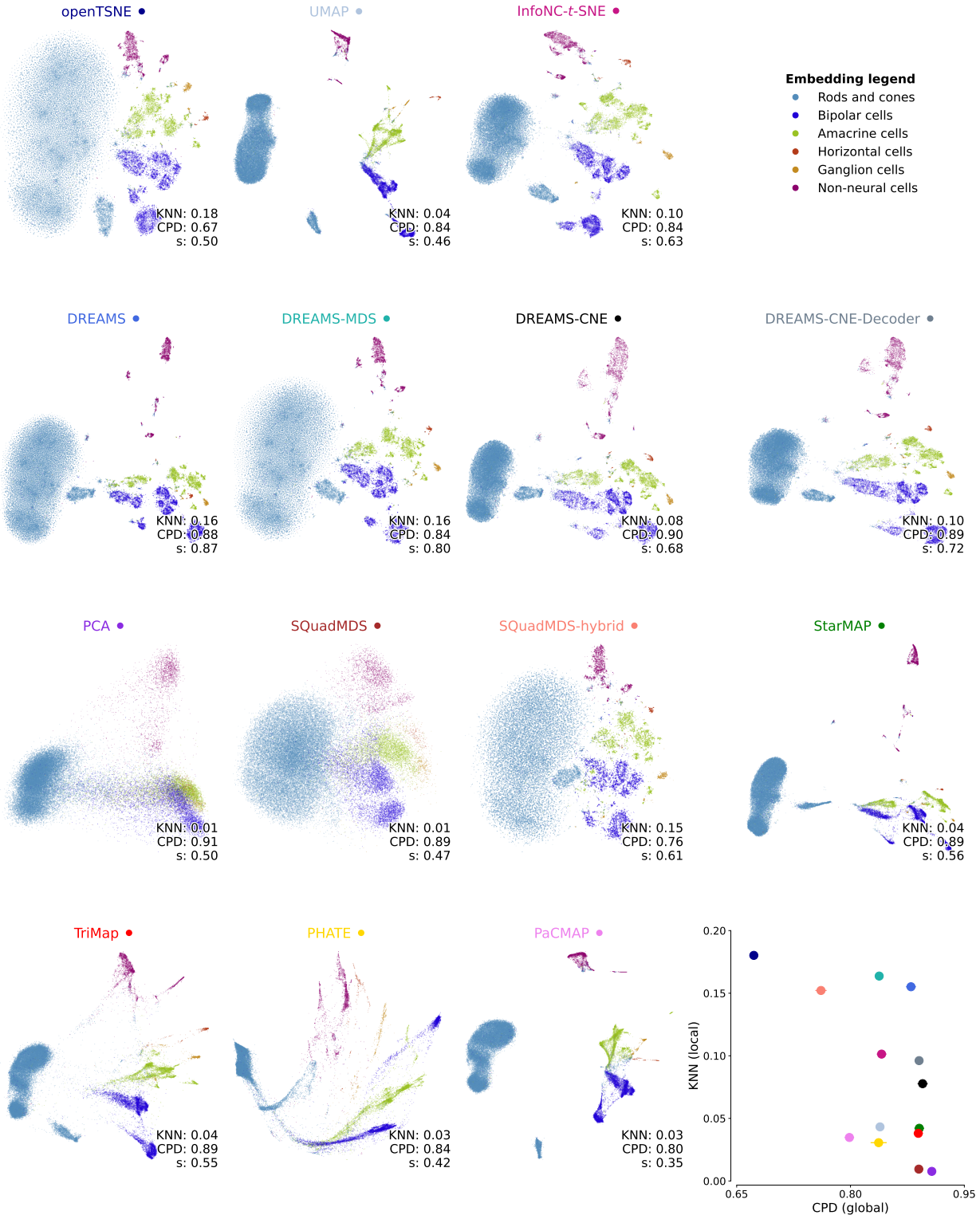

Figure S7: Visualizations of the Macosko et al. dataset with all considered methods.

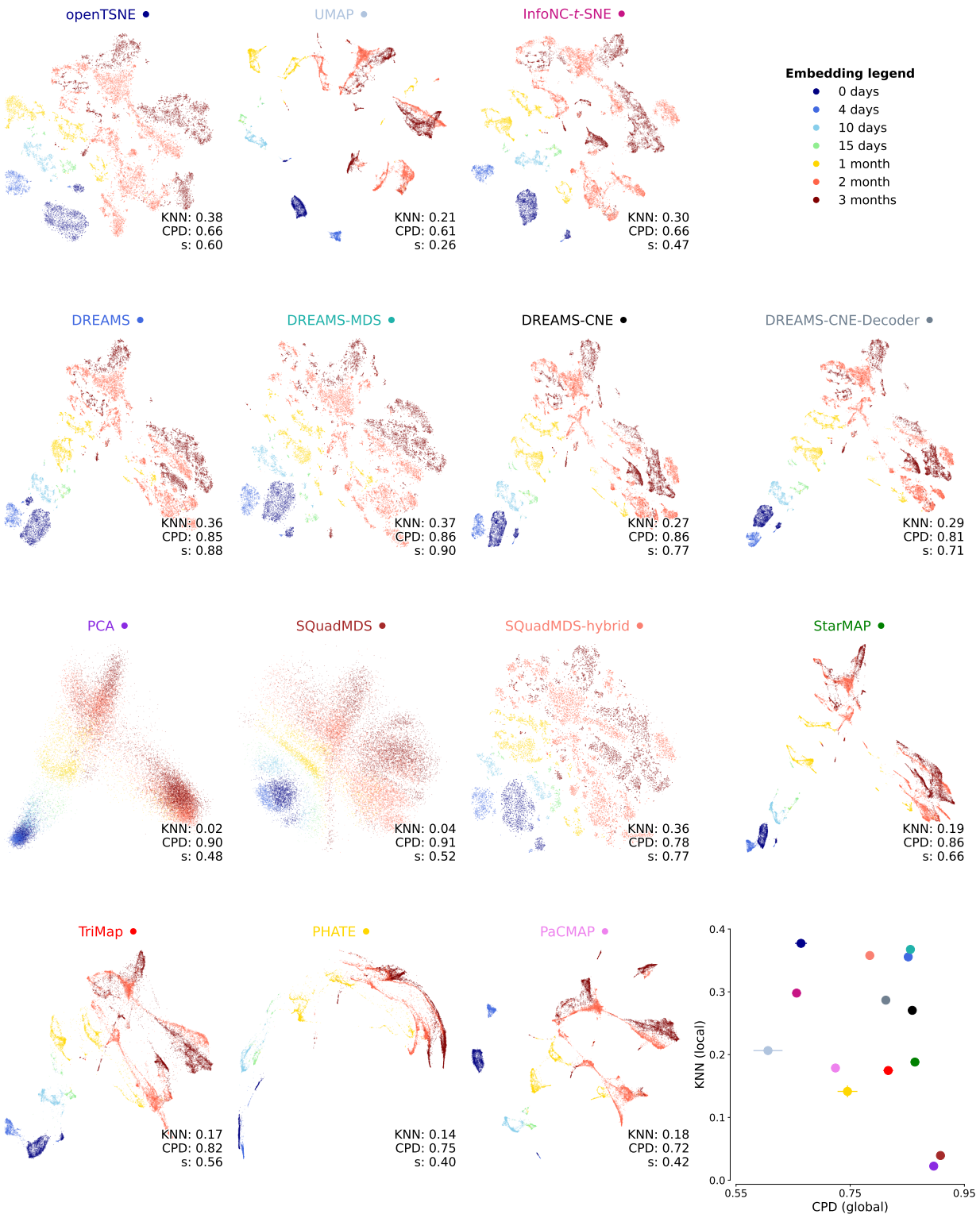

Figure S8: Visualizations of the Kanton et al. dataset with all considered methods.

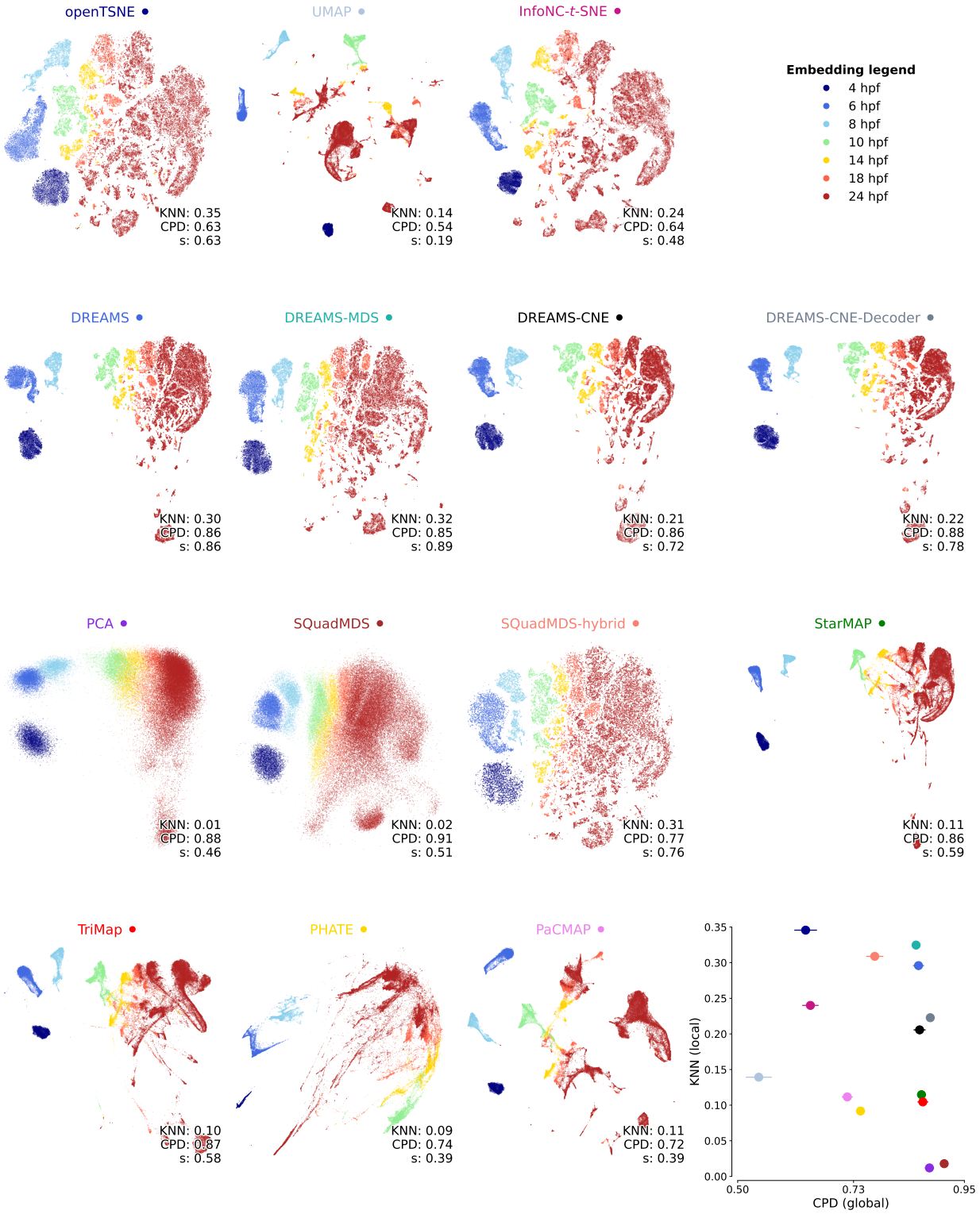

Figure S9: Visualizations of the Wagner et al. dataset with all considered methods (hpf = hours post fertilization).

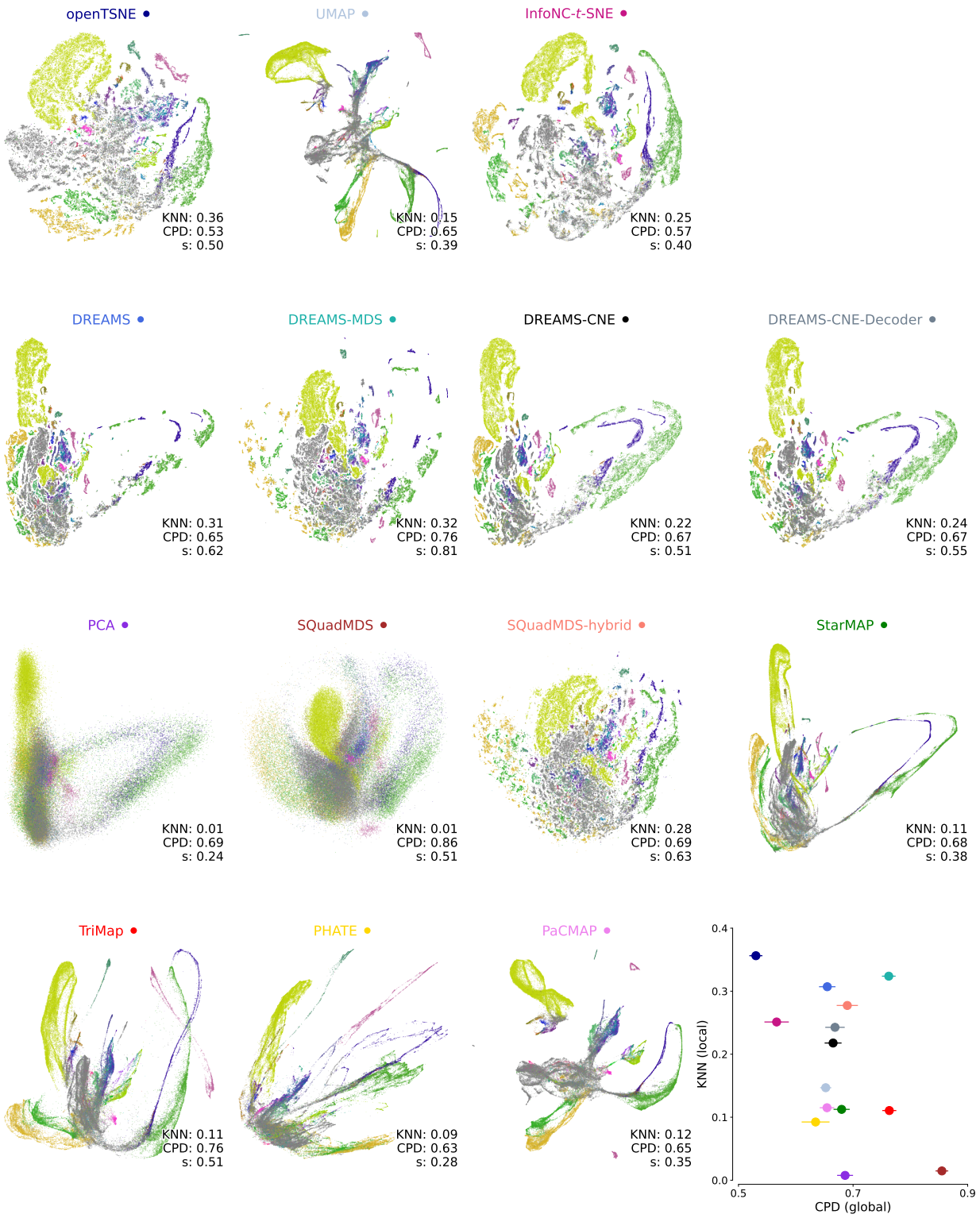

Figure S10: Visualizations of the Packer et al. dataset with all considered methods.

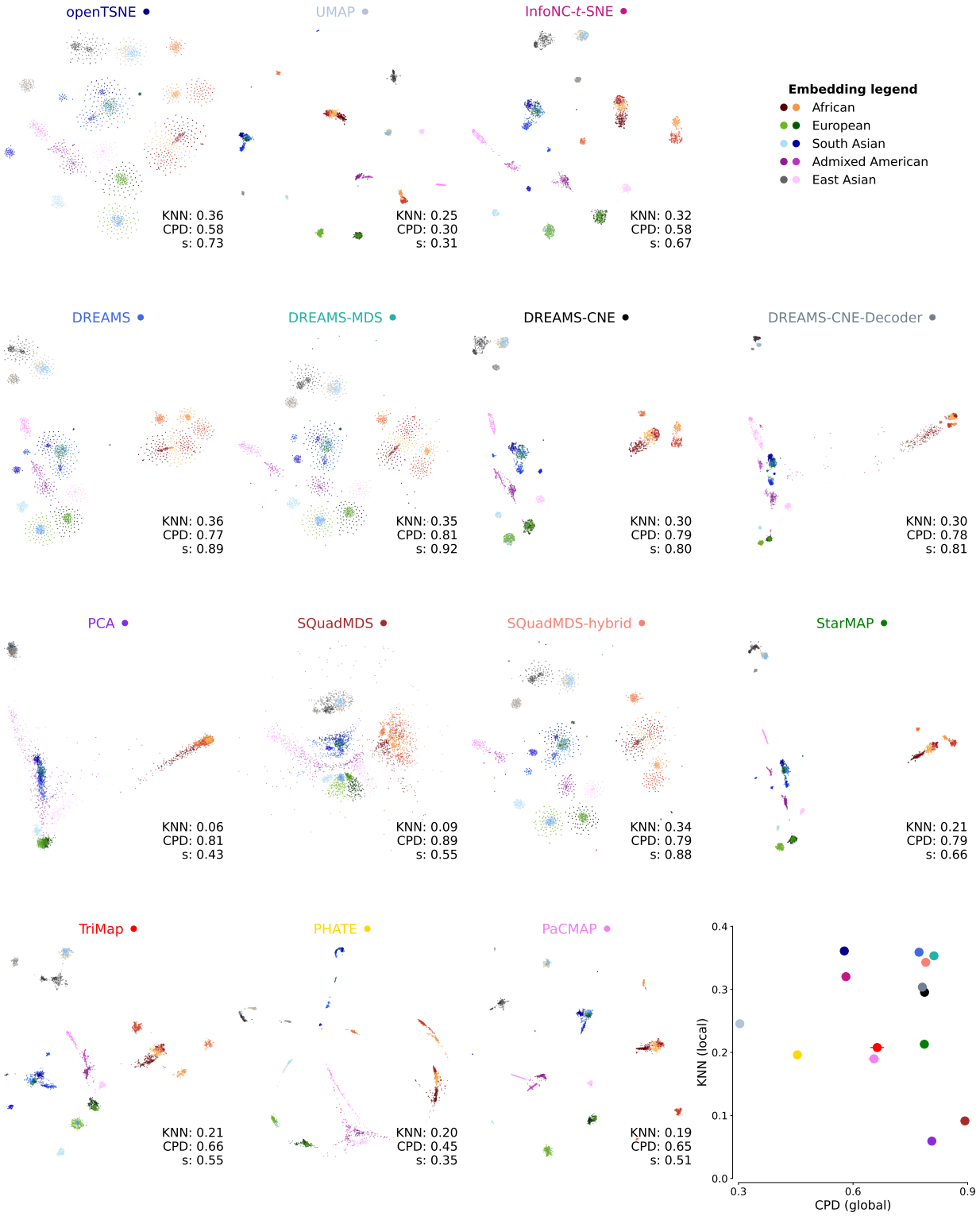

Figure S11: Visualizations of the 1000 Genomes Project dataset (The 1000 Genomes Project Consortium, 2015) with all considered methods.

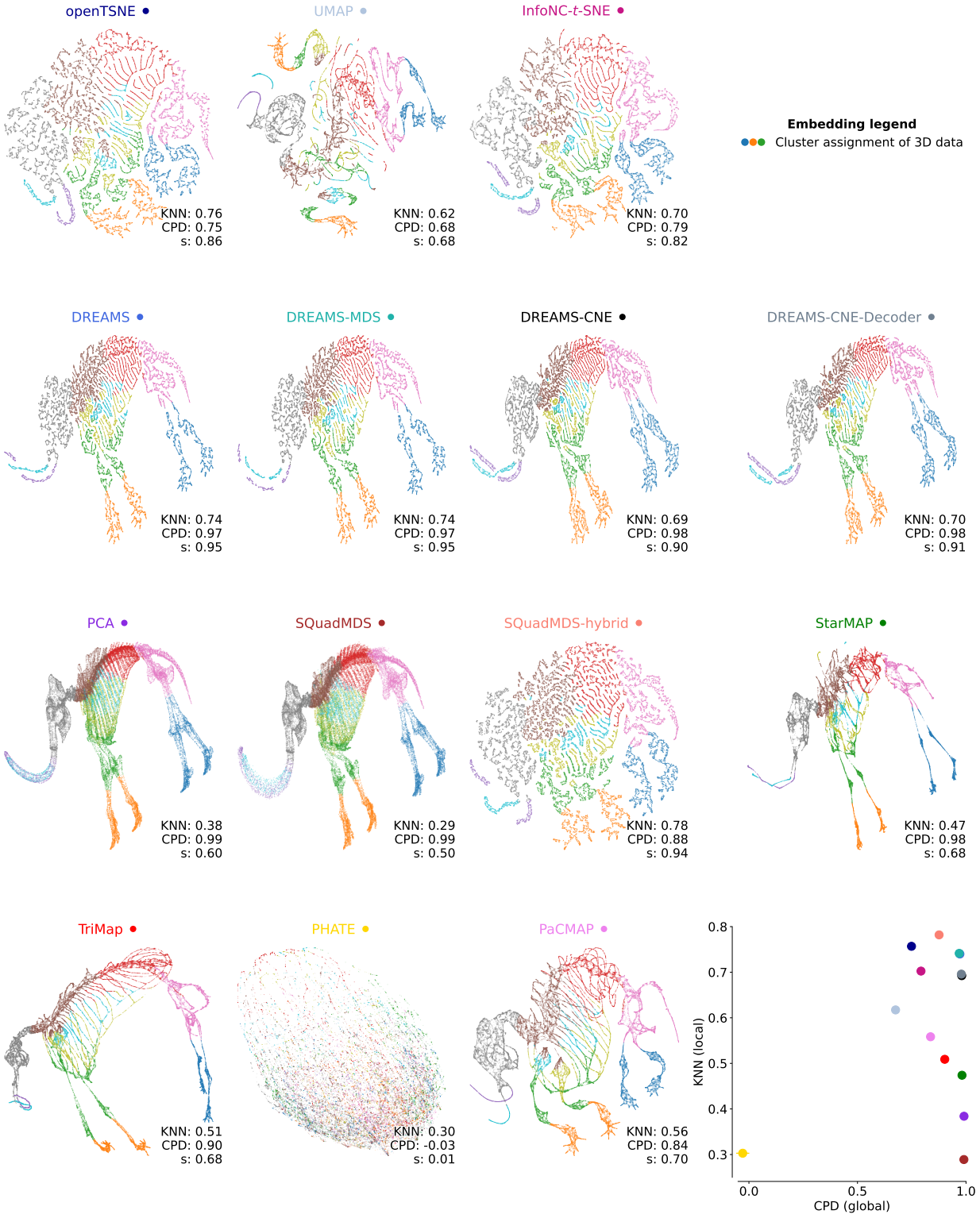

Figure S12: Visualizations of the Mammoth dataset (Smithsonian Institution, 2020; Noichl, 2025) with all considered methods. Colors represent cluster assignment of original data and are used for visual clarity but do not correspond to any ground truth labels.

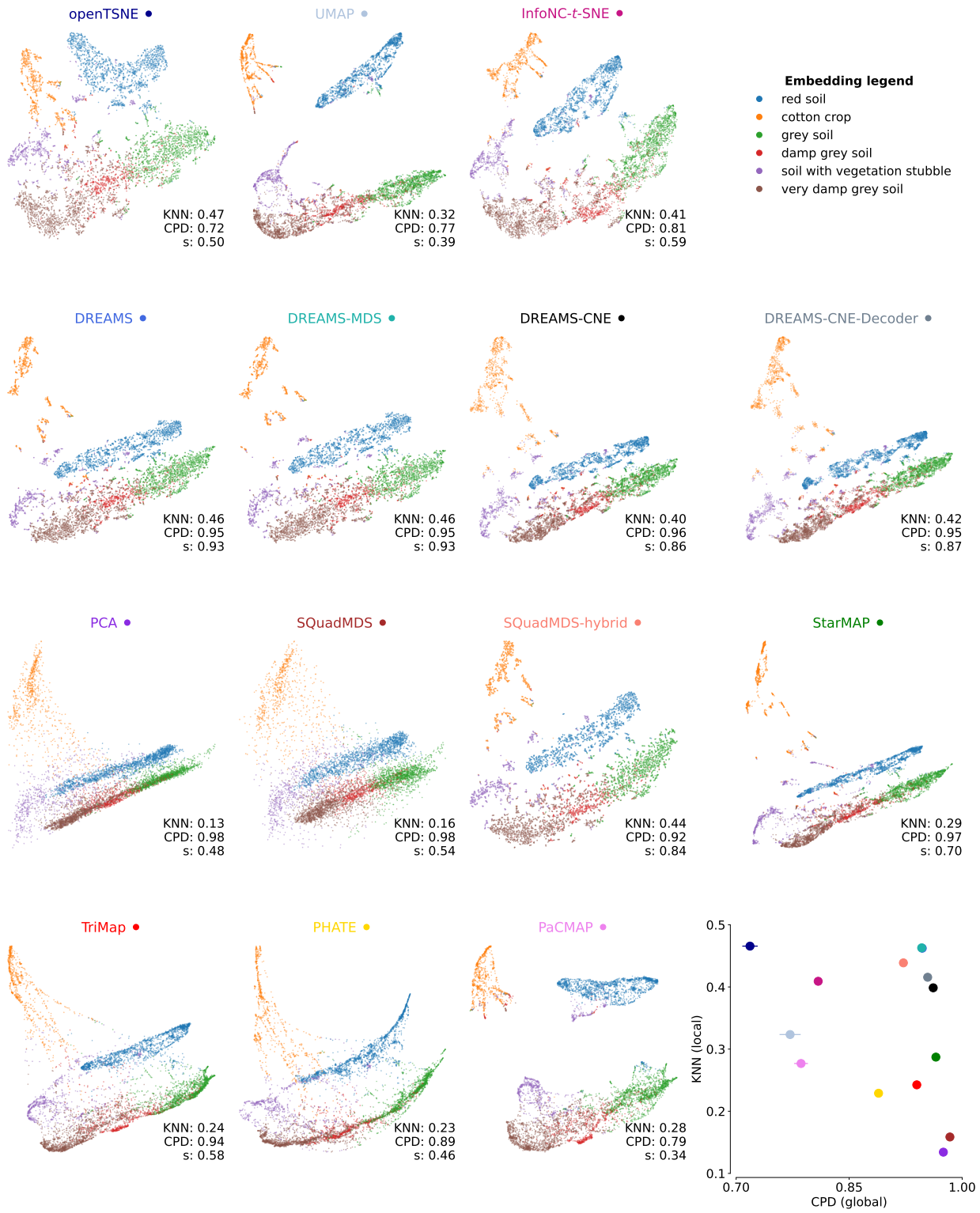

Figure S13: Visualizations of the Landsat Satellite dataset (Srinivasan, 1993) with all considered methods.

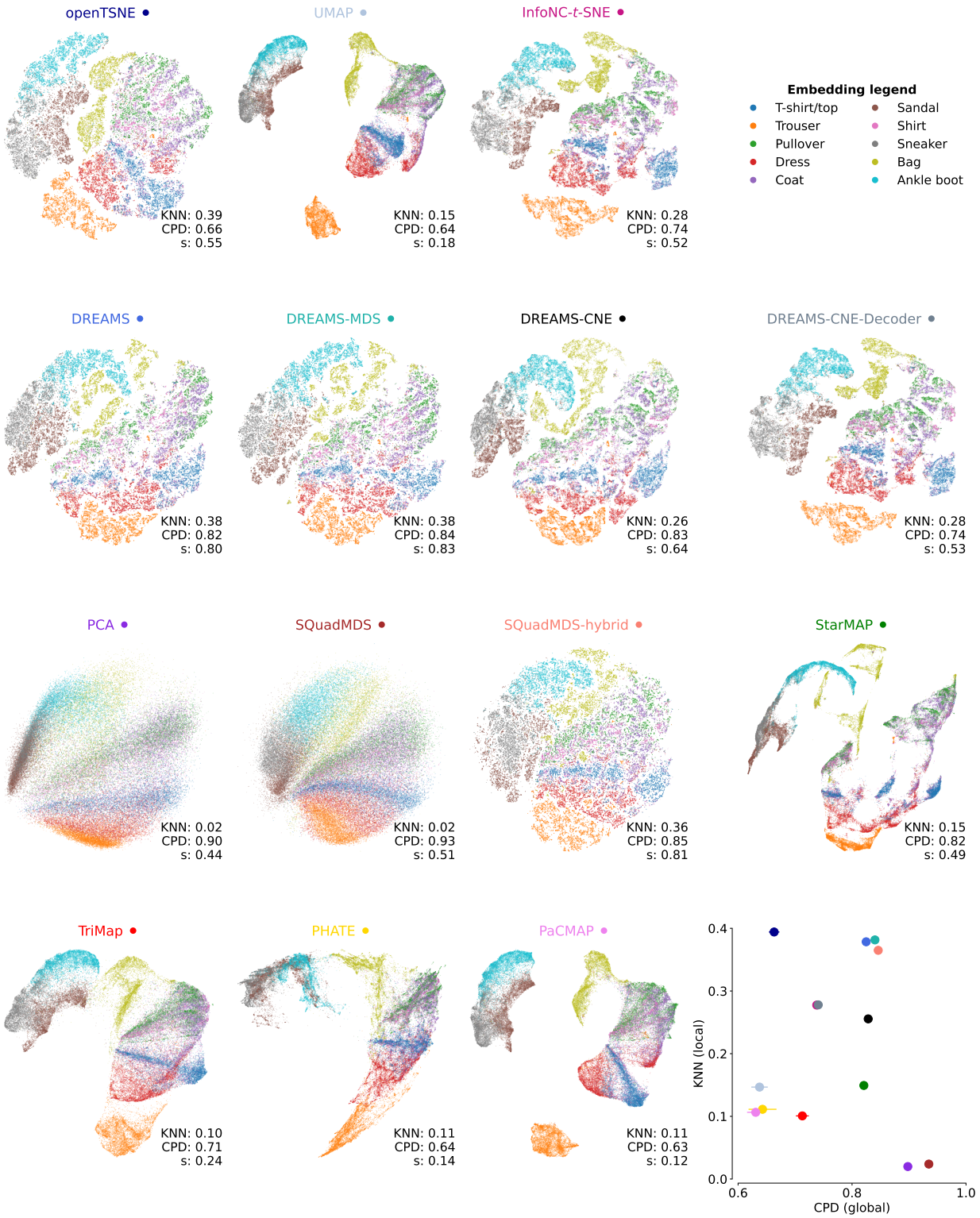

Figure S14: Visualizations of the Fashion MNIST dataset (Xiao et al., 2017) with all considered methods.

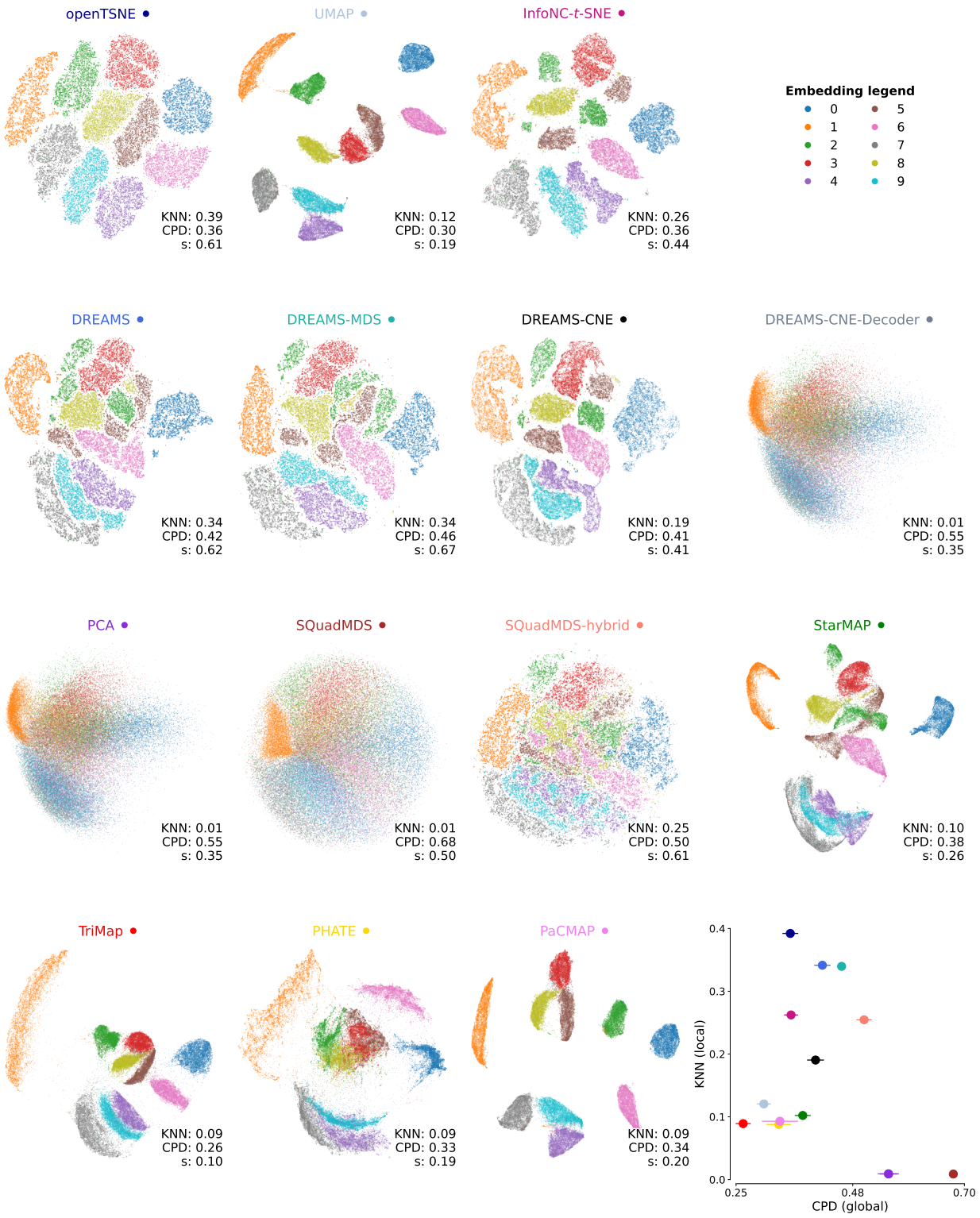

Figure S15: Visualizations of the MNIST dataset (Lecun et al., 1998) with all considered methods.

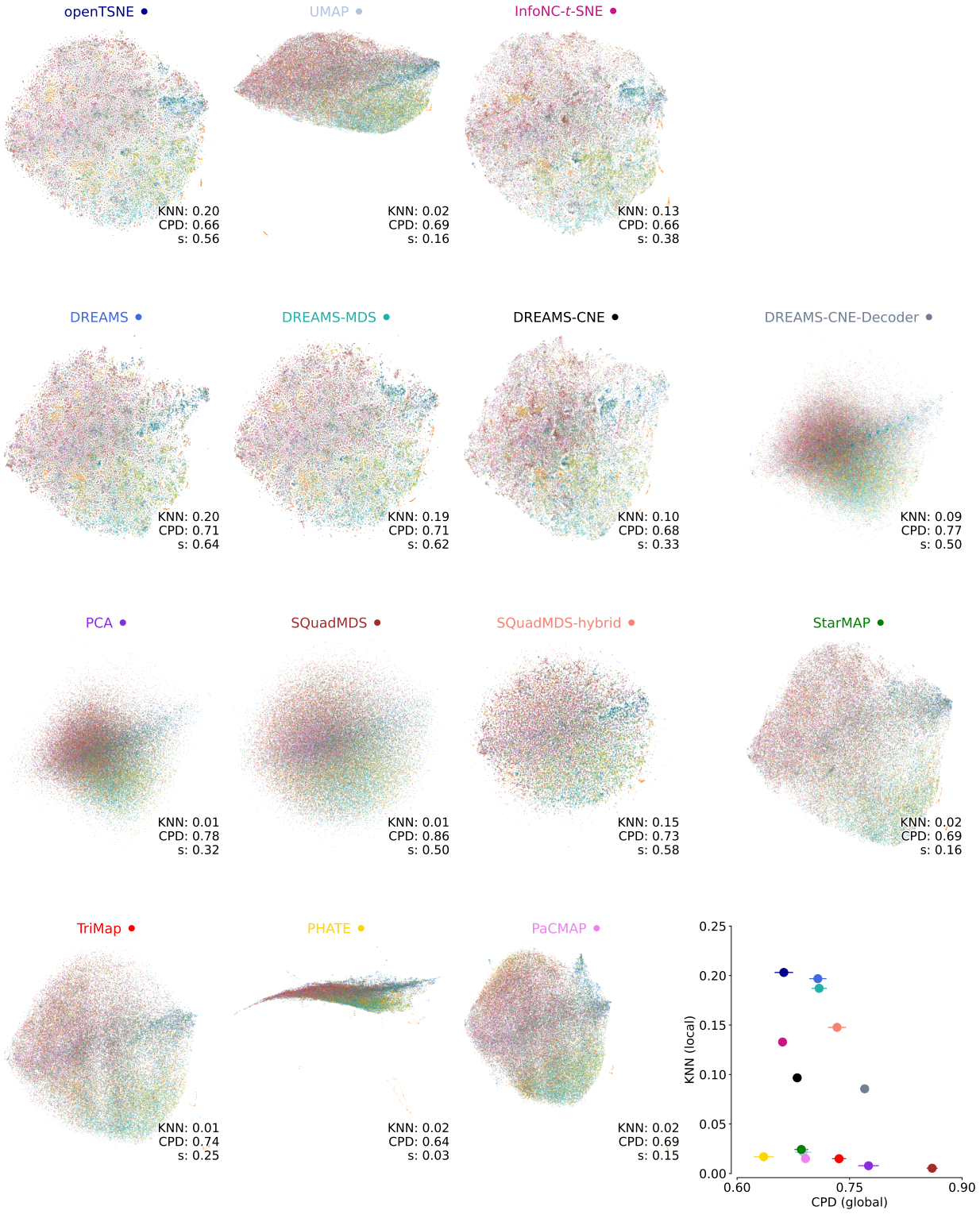

Figure S16: Visualizations of the CIFAR10 dataset (Krizhevsky et al., 2009) with all considered methods.